The Journal of Physiology

Deep phenotyping of cardiac function in heart transplant patients using cardiovascular system models

Amanda L. Colunga[1,*], Karam G. Kim[2,*], N. Payton Woodall[1,*], Todd F. Dardas[2], John H. Gennari[2], Mette S. Olufsen[1] and Brian E. Carlson[3]

[1] *North Carolina State University, Raleigh, North Carolina, United States*
[2] *University of Washington, Seattle, Washington, United States*
[3] *University of Michigan, Ann Arbor, Michigan, United States*

Edited by: Don Bers & Jolanda Van der Velden

Key points

- Right heart catheterization data from clinical records of heart transplant patients are used to identify patient-specific models of the cardiovascular system.
- These patient-specific cardiovascular models represent a snapshot of cardiovascular function at a given post-transplant recovery time point.
- This approach is used to describe cardiac function in 10 heart transplant patients, five of which had multiple right heart catheterizations allowing an assessment of cardiac function over time.
- These patient-specific models are used to predict cardiovascular function in the form of right and left ventricular pressure-volume loops and ventricular power, an important metric in the clinical assessment of cardiac function.
- Outcomes for the longitudinally tracked patients show that our approach was able to identify the one patient from the group of five that exhibited post-transplant cardiovascular complications.

Abstract Heart transplant patients are followed with periodic right heart catheterizations (RHCs) to identify post-transplant complications and guide treatment. Post-transplant positive outcomes are associated with a steady reduction of right ventricular and pulmonary arterial pressures, toward normal levels of right-side pressure (about 20 mmHg) measured by RHC. This study shows that more information about patient progression is obtained by combining standard RHC measures with mechanistic computational cardiovascular system models. The purpose of this study is twofold: to understand how cardiovascular system models can be used to represent a patient's

Amanda Lee Colunga was raised in Miami, FL, and earned her Bachelor of Science in Applied Mathematics at Florida State University followed by her Master of Science in Applied Mathematics at North Carolina State University. She is now currently working on her PhD and hopes to use her mathematical knowledge and physiological interests to further her career in biological modelling and data analysis. **Graham Karam Kim** was born in Seoul, South Korea and grew up in Portland, Oregon. He earned his Bachelor of Science in Bio and Brain Engineering from the Korea Advanced Institute of Science and Technology. In 2013, he moved to Seattle, WA, to pursue his interests in the secondary usage of biomedical data. He earned his Doctor of Philosophy in Biomedical and Health Informatics from the University of Washington in 2018. **N. Payton Woodall** earned his Bachelor of Science in Mathematics at North Carolina State University and now works as a Programming Specialist at Nuventra Inc. where he uses his mathematical and physiological knowledge in the field of pharmacokinetic and pharmacodynamic research. Payton hopes to pursue an advanced degree to further develop his career in biological modelling to research new ways that organ systems can be analysed non-invasively.

*Authors contributed equally to this manuscript

This article was first published as a preprint. Colunga AL, Kim KG, Woodall NP, Dardas TF, Gennari JH, Olufsen MS, Carlson BE.2018.Deep phenotyping of cardiac function in heart transplant patients using cardiovascular systems models. arXiv. https://arxiv.org/abs/1812.11857.

 DOI: 10.1113/JP279393

cardiovascular state, and to use these models to track post-transplant recovery and outcome. To obtain reliable parameter estimates comparable within and across datasets, we use sensitivity analysis, parameter subset selection, and optimization to determine patient-specific mechanistic parameters that can be reliably extracted from the RHC data. Patient-specific models are identified for 10 patients from their first post-transplant RHC, and longitudinal analysis is carried out for five patients. Results of the sensitivity analysis and subset selection show that we can reliably estimate seven non-measurable quantities; namely, ventricular diastolic relaxation, systemic resistance, pulmonary venous elastance, pulmonary resistance, pulmonary arterial elastance, pulmonary valve resistance and systemic arterial elastance. Changes in parameters and predicted cardiovascular function post-transplant are used to evaluate the cardiovascular state during recovery of five patients. Of these five patients, only one showed inconsistent trends during recovery in ventricular pressure–volume relationships and power output. At the four-year post-transplant time point this patient exhibited biventricular failure along with graft dysfunction while the remaining four exhibited no cardiovascular complications.

(Received 9 December 2019; accepted after revision 1 May 2020; first published online 5 May 2020)
Corresponding author Brian E. Carlson: University of Michigan, 2800 Plymouth Road, NCRC B10/A126, Ann Arbor, Michigan, 48109, United States. Email: bcarl@umich.edu

Introduction

Diagnosis and treatment plans for patients with cardiovascular pathophysiologies are currently being guided with an increasing number of non-invasive and minimally invasive clinical measures by statistically inferring correlations between measurements and diagnosis/treatment. However, this approach is limited in scope since the underlying physiological mechanisms associated with the success or failure of a given treatment for a given patient cannot be discriminated. One example is the assessment of cardiovascular function using right heart catheterization (RHC) measurements after heart transplants. For this patient group, repeated RHC measurements of ventricular and pulmonary arterial pressure are used to monitor post-transplant pulmonary hypertension, which if not resolved, can lead to complications in post-transplant recovery (Greenberg *et al.* 1985; Bhatia *et al.* 1987; Young *et al.* 1987; Goland *et al.* 2007). Traditionally, RHC measurements are used to inform post-transplant treatment and intervention and a close monitoring of these measurements has been associated with better outcomes. However, these RHC measurements only describe the upper-level phenotype of the cardiovascular system and do not explicitly take advantage of the relationships between pressure, volume and flow governed by the known physiology of the cardiovascular system. It has been suggested (Armitage *et al.* 1987; Stobierska-Dzierzek *et al.* 2001) that a complete evaluation of the cardiovascular system could improve the detection and treatment of dysfunction in the transplanted heart. The study presented here builds a patient-specific computational methodology (Fig. 1) integrating clinical measures and computing time-varying patient-specific pressures, flows and volumes, while estimating mechanistic parameters, which can be incorporated into clinical analyses to guide treatment and assess the recovery of heart transplant patients. Many of the estimated mechanistic parameters and predicted cardiovascular variables obtained with the computational approach presented here cannot easily be measured in the clinic.

In addition to the RHC measurements, echocardiography, magnetic resonance and Doppler imaging have been used to track the metrics of post-transplant cardiac function (Sundereswaran *et al.* 1998; Dandel *et al.* 2001; Marie *et al.* 2001; Sun *et al.* 2005). These non-invasive modalities are always coupled with RHC measurements in standard clinical protocols and may not on their own provide sufficient information needed to improve diagnosis and treatment protocols. The study by Dandel *et al.* (2001) utilized tissue Doppler, to determine the optimal times that RHC measurements should be made during recovery, while the other studies focused on identifying a single biomarker or set of biomarkers from echocardiography which were used to identify dysfunction and guide therapy. This latter approach is problematic in two ways. First, if a prospective biomarker or set of biomarkers does not discriminate outcomes, another biomarker or set of biomarkers must be selected, and the process repeated. Second, this approach ignores the fact that post-transplant recovery and outcome are multifactorial, involving the function of the entire cardiovascular system working in conjunction with the transplanted heart and thus biomarkers focusing only on the transplanted heart have a reduced chance of discriminating patient outcome.

To gain more insight into post-transplant recovery of cardiovascular function, our approach uses mathematical models to analyse deidentified RHC data from patient

electronic health records (EHRs) that also contain post-transplant clinical outcomes. More specifically, we employ a mechanistic representation of each patient at each specific recovery time point using a mathematical model of the cardiovascular system similar to several previously developed models (Smith *et al.* 2004; Lumens *et al.* 2009; Beard *et al.* 2013; Williams *et al.* 2014). We personalize the model by calculating initial estimates of model parameters using information extracted from the EHR. Next, we use rigorous model analysis techniques to identify and estimate parameters, minimizing the least squares error between the model predictions and data. The final step involves running forward simulations with the personalized instance of the model predicting patient-specific dynamics that can be used to inform the clinical diagnosis and treatment procedure. A vital part of this analysis is to select the right granularity of the model informed by the clinical data, and then quantify which parameters can be estimated given the model and available RHC data. At this point the RHC data used here does not contain any pressure waveforms and is not combined with any direct measures of left ventricular function.

The patient-specific instantiations of the mathematical model are used to infer the underlying differences between 10 patients, and then associate how changes in cardiovascular function are related to clinical outcome. By integrating our physiological knowledge of the cardiovascular system with patient-specific data, we are constraining the system to represent the cardiovascular state of an individual patient. In addition, since this is a retrospective analysis, our approach makes it possible to search for early indicators of positive and negative heart transplant outcomes.

Of the 10 patients' datasets obtained, five contain longitudinal RHC measurements at an additional 3–7 post-transplant time points over the span of up to 13 months. We analyse these longitudinal RHC measures from these patients to quantify how underlying cardiovascular function for each of these five patients is changing during post-transplant recovery. Finally, the trends in the predictions of pressure-volume (PV) loops and ventricular power output for the right and left ventricle are associated with clinical outcome in each of these five patients.

Patient 572					
$P_{rv,syst}$	31	$P_{sa,syst}$	116		
Patient 558					
$P_{rv,syst}$	30.5	$P_{sa,syst}$	114	66	
Patient 266				100	
$P_{rv,syst}$	37	$P_{sa,syst}$	154	49	82
Patient 233				90	180
$P_{rv,syst}$	40	$P_{sa,syst}$	149	81	101
$P_{rv,diast}$	4	$P_{sa,diast}$	83	90	170
$P_{pa,syst}$	34	*Heart Rate*	83	75	F
$P_{pa,diast}$	14	*Weight*	96	169	
P_{wedge}	11	*Height*	172	M	
Cardiac Output	6	*Sex*	F		

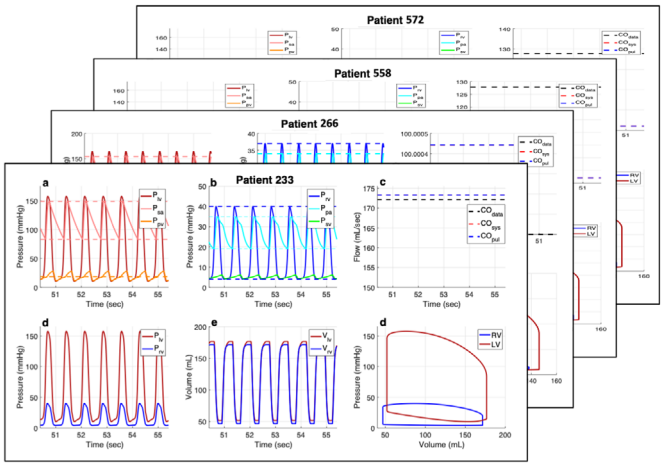

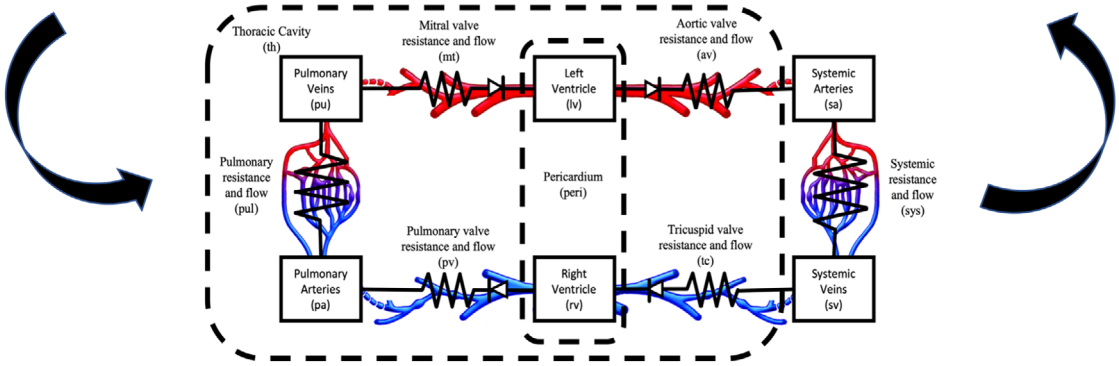

Figure 1. Workflow showing patient-specific modeling of cardiovascular function
Retrospective approach where electronic health record data is used to identify a mechanistic model of the closed loop cardiovascular system thus generating model versions representing the cardiovascular function of each patient (or patient at different times). These patient-specific instantiations of the model can then be used to understand differences between the outcomes across populations of patients.

Methods

RHC measures

This study analyses 10 RHC records from heart transplant patients extracted from the clinical data repository at the University of Washington Medicine Regional Heart Center. This retrospective data capture was approved by the Institutional Review Board (IRB) at the University of Washington and the requirement of informed consent was waived for the use of the deidentified clinical repository data used within this study. The data in the repository were exported from the Mac-Lab Hemodynamic Recording System (GE Healthcare, Chicago, IL, USA) used in the University of Washington cardiac catheterization lab. The repository was queried for RHC datasets from heart transplant patients with catheterization procedures performed between 6 March 2014 and 21 March 2016. Ten patient records were retrieved; of these, five records contained multiple RHC measures from a period of 4–12 months immediately following the transplant. The datasets contained 12 clinically measured values: systolic and diastolic pressure measured in the right ventricle, pulmonary artery, and systemic arteries; an average pulmonary capillary wedge pressure, heart rate, cardiac output, body weight, height and sex, as shown in Table 1.

Mathematical model

Inspired by a previously published cardiovascular system-level model (Smith *et al.* 2004), we developed the mechanistic model used here (schematic shown in Fig. 2) to study patient-specific cardiovascular function in heart transplant patients. The objective of this study is to create a simple model that can simulate the RHC and systemic arterial blood pressure data. The main differences between our model and the model by Smith *et al.* are that (1) we ignored the right ventricular and left ventricular pressures' and volumes' influence on each other via the septal wall otherwise known as ventricular–ventricular interaction (VVI) and (2) we omitted the influence of the inertance of blood flowing through the four heart valves. We justified the former using simple sensitivity analysis by doubling and halving the parameters involved with VVI around nominal values for several of our patients. Low sensitivity of the parameters involved with VVI did not justify the significant increase in model complexity. This observation agrees with findings in the literature, which note that VVI mainly impacts left ventricular dynamics for patients with very high right ventricular pressures and volumes associated with severe pulmonary hypertension (Maughan *et al.* 1981; Gan *et al.* 2006). Inertance of blood flowing through the four valves in the heart could be important for the prediction of waveforms (especially the aortic pressure waveform). However, the RHC measures used here are not given as waveforms in the EHR but are simply provided as maximal and minimal pressures in systole and diastole, respectively. Therefore, the RHC data from the EHRs do not contain the information needed to identify inertance parameters.

The cardiovascular systems model depicted in Fig. 2 is used to predict blood pressure, flow, and volume in the heart's left and right ventricles, and the pulmonary and systemic arteries and veins. The model is analogous to several resistor-capacitor electrical components in series where current is analogous to blood flow Q (ml·s^{-1}), voltage to pressure P (mmHg), and charge to volume V (ml). Note, the blood flow Q is directly related to cardiac output which is the average flow over the period, T, of the cardiac cycle, i.e. CO $= \frac{1}{T}\int_0^T Q\ dt$ (ml·s^{-1}). In addition, elastance E (mmHg·ml^{-1}) is the reciprocal of compliance, which is analogous to capacitance, while R (mmHg·s·ml^{-1}) represents the resistance to flow within a compartment. Diodes are used to simulate one-way valves preventing blood from exiting a ventricle through a closed aortic, mitral, pulmonary or tricuspid heart valve. The muscle contraction within the heart is modelled using a Gaussian activation function defined over one cardiac cycle as

$$A(\tilde{t}) = e^{-a(\tilde{t}-T/2)^2}, \tag{1}$$

where a is a scaling factor with the value of heart rate from Table 1 and units of 1 s^{-2} to make the exponent unitless, $T = 1/H$ (s), where H is heart rate in beats per second, is the period of the cardiac cycle and $\tilde{t} = mod(\mathrm{t}, T)$ (s) is the time from the start of the current cardiac cycle. This relationship creates a symmetrical curve about $T/2$ bounded by $0 \leq A(\tilde{t}) \leq 1$ and denotes the relative contribution of the systolic and diastolic pressure development during the cardiac cycle. The end-systolic pressure P_{es} and volume V_{es} in the left and right ventricles are assumed to be linearly related to the end-systolic ventricular elastance E_{es} via

$$P_{es} = E_{es}\,(V_{es} - V_d)\,, \tag{2}$$

where V_d is the end-systolic volume at zero pressure. In addition, the end-diastolic pressure P_{ed} is related non-linearly to the end-diastolic volume V_{ed} by

$$P_{ed} = P_0\left[e^{\lambda(V_{ed}-V_0)} - 1\right], \tag{3}$$

where P_0 is the pressure at the unstressed volume V_0, and λ (ml^{-1}) specifies the steepness of the exponential PV relationship in diastole. The pressure in the left ventricle at any time in the cardiac cycle is calculated by combining eqns (2) and (3) giving

$$P(t) = A(\tilde{t})P_{es} + [1 - A(\tilde{t})]\,P_{ed} + P_{th}, \tag{4}$$

Table 1. Right heart catheter measurements extracted from the clinical data repository at the University of Washington Medicine Regional Heart Center

Patient	P_{rv} systole	P_{rv} diastole	P_{pa} systole	P_{pa} diastole	P_{pcw} average	P_{sa} systole	P_{sa} diastole	CO** (L/min)	HR** (bpm)	Weight (kg)	Height (cm)	Sex
060	36	2	36*	14	16	132	79	6.3	69	62	180	M
066	28	1	26	13	8	134	79	7.8	81	120	194	M
233	40	4	35	19	19	149	83	10.3	83	96	172	F
266(1)	37	10	34	14	11	154	81	6.0	90	75	169	M
266(2)	30	6	27	10	9	121	75	6.5	94	71	169	M
266(3)	29	9	30*	13	12	115	82	6.1	96	73	169	M
266(4)	27	8	25	10	9	112	69	5.2	92	73	169	M
266(5)	23	5	26*	10	8	106	77	5.4	94	75	169	M
266(6)	27	9	28*	12	11	119	81	5.9	101	79	169	M
266(7)	22	5	22*	8	7	107	76	6.0	102	75	169	M
363(1)	30	7	29*	20	12	108	78	4.8	109	80	162	M
363(2)	22	1	21	13	6	119	87	4.1	92	75	162	M
363(3)	25	2	25*	17	10	113	73	3.4	108	79	162	M
363(4)	26	1	24	12	7	107	85	4.8	119	79	163	M
456(1)	44	4	35	13	16	104	67	5.5	90	78	170	M
456(2)	42	4	36	14	15	122	75	5.0	86	78	170	M
456(3)	39	2	33	14	13	128	88	4.6	93	75	170	M
456(4)	23	5	24*	13	6	130	79	5.0	108	78	170	M
456(5)	37	11	33	18	15	118	78	5.9	93	78	170	M
456(6)	34	12	31	18	14	133	75	5.5	103	73	170	M
456(7)	30	4	24	13	9	110	74	4.7	99	78	170	M
456(8)	28	1	24	9	6	99	63	6.9	100	74	170	M
558(1)	31	3	32*	15	14	114	49	7.7	90	101	170	F
558(2)	38	7	33	12	15	124	77	6.1	63	101	170	F
558(3)	34	5	33	14	18	144	85	7.9	71	101	170	F
558(4)	36	1	35	12	16	152	88	7.8	73	103	170	F
558(5)	45	5	44	21	25	125	71	7.8	70	110	170	F
558(6)	28	1	27	10	12	128	79	7.4	69	103	170	F
558(7)	33	2	34*	17	12	166	102	7.4	69	103	170	F
572(1)	31	5	30	12	12	116	66	6.4	100	82	180	M
572(2)	29	5	24	7	9	119	72	7.3	97	82	180	M
572(3)	26	2	24	8	7	112	72	6.7	100	82	180	M
572(4)	26	2	23	10	9	109	71	6.5	95	82	180	M
572(5)	28	1	24	10	9	112	73	6.9	90	82	180	M
572(6)	17	4	20*	10	10	108	67	6.2	88	83	180	M
572(7)	22	1	16	9	5	122	71	7.1	98	82	180	M
572(8)	19	4	17	9	7	115	73	7.2	97	82	180	M
794	38	6	39*	17	21	98	57	6.8	84	44	174	F
839	25	1	18	9	7	135	84	6.1	91	83	170	M

All pressures are given in mmHg. * indicates that when nominal values were calculated, pulmonary artery pressure was adjusted to be 95% of the pressure in the right ventricle to enforce a pressure drop in the direction of flow. **Measurements of cardiac output (CO) and heart rate (HR) are given in conventional units (l min^{-1}) and (bpm), but to keep consistency of units, in the model these are converted to (ml/s) and (bps). Superscripts on patient number indicates different RHC measurements for a given patient at sequential recovery timepoints. Subscripts: *rv* – right ventricle, *pa* – pulmonary arteries, *pcw* – pulmonary capillary wedge, *sa* – systemic arteries

where $P_{th} = 0$ is the assumed tissue pressure in the thoracic cavity. As $A(\tilde{t})$ changes throughout the cardiac cycle, eqn (4) shifts the contributions of the systolic and diastolic pressure terms to give the total pressure in the ventricle. When $A(\tilde{t})$ is equal to 1 the pressure is described solely by eqn (2) and when equal to 0 by the diastolic PV curve of eqn (3). Since the pulmonary arteries and veins are located in the thoracic cavity, the pressure and volume are related as

$$P = EV + P_{th}, \tag{5}$$

while the majority of the systemic arteries and veins are outside the thoracic cavity where

$$P = EV. \tag{6}$$

Blood flow in and out of each compartment is proportional to the difference between the compartment's input and output pressures and represented by the fluid equivalent to Ohm's Law

$$Q = \frac{P_{in} - P_{out}}{R} \tag{7}$$

and conservation of volume, where the change in the compartmental volume must equal the difference in flow in and flow out, implying that

$$\frac{dV}{dt} = Q_{in} - Q_{out} \tag{8}$$

for each compartment. To model the one-way heart valves, we set flow to zero when pressure across the valve indicates the valve is closed, giving

$$Q_{valve} = \begin{cases} \frac{P_{in}-P_{out}}{R} & \text{if } P_{in} > P_{out} \\ 0 & \text{otherwise} \end{cases} \tag{9}$$

for the aortic (av), tricuspid (tc), pulmonary (pv), and mitral (mt) valves. A list of equations making up the model is given in Appendix A, and a version of the model implemented in MATLAB (The MathWorks, Inc., Natick, MA) is available at github.com/alcolunga/Heart_Tx_CVS_Model and at https://wp.math.ncsu.edu/cdg/publications/.

In summary, the system of equations can be written in the form

$$\frac{dx}{dt} = f(x, t:\theta)$$
$$y = g(x, t:\theta)$$
$$x = \{V_{lv}, V_{sa}, V_{sv}, V_{rv}, V_{pa}, V_{pu}\}$$
$$\theta = \{E_{lv}, V_{d,lv}, P_{0,lv}, \lambda_{lv}, V_{0,lv}, E_{rv}, V_{d,rv}, P_{0,rv}, \lambda_{rv}, V_{0,rv}, E_{pa}, E_{pu}, R_{pul}, P_{th}, E_{sa}, E_{sv}, R_{sys}, R_{mt}, R_{av}, R_{tc}, R_{pv}\}$$
$$y = \{P_{rv}, P_{pa}, P_{pu}, P_{sa}, Q\}.$$

Where x are the state variables of the model, t is time, θ are the model parameters and y are the model outputs, of which we take the maximum, minimum or average in order to compare with our clinical data. The data are expected to match model output as

$$y_i^d = y(t_i) + \varepsilon_i,\ i = 1, \ldots, K,$$

where K denotes the number of time points, and ε_i is the error assumed to be independent identically distributed random variables with mean $E[\varepsilon_i] = 0$, covariance $\mathrm{cov}(\varepsilon_i, \varepsilon_j) = 1$, and constant variance $var(\varepsilon_i) = \mu^2$. The equations are solved under the assumptions that the cardiac cycle is initialized to be at end-diastole, i.e. the volumes in the left and right heart are at their maximum, while the venous and arterial volumes are initialized at their average values.

Nominal parameter values

Nominal parameter values for each patient RHC are determined from the clinical data and literature values using an approach similar to a previous method for the rat cardiovascular system (Marquis *et al.* 2018) but translated to the human. The nominal parameters and how they are obtained are shown in Table 2.

Blood volume

In order to compute nominal values of all elastances, the blood volume distribution in the cardiovascular system must be estimated. Total blood volume (TBV in ml) (Nadler *et al.* 1962) and body surface area (BSA in m^2) (Du Bois & Du Bois, 1916) are calculated as functions of height (Hgt in cm), weight (BW in kg), and sex as

$$\mathrm{TBV} = \begin{cases} \left(0.3669\ \mathrm{Hgt}^3 + 0.03219\ \mathrm{BW} + 0.641\right)\ 1000 \\ \qquad \text{for males} \\ \left(0.3561\ \mathrm{Hgt}^3 + 0.03308\ \mathrm{BW} + 0.1833\right)\ 1000 \\ \qquad \text{for females} \end{cases} \tag{10}$$

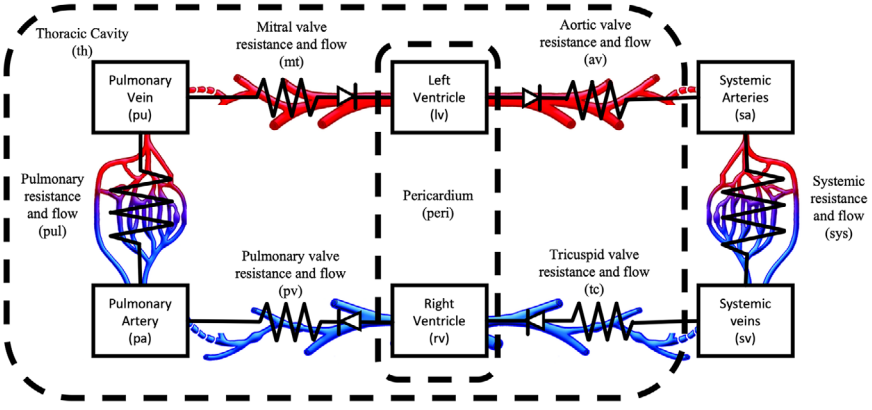

Figure 2. Schematic of closed loop cardiovascular model used in this study
In the model by Smith *et al.* (2004) left and right ventricles interact by accounting for the dynamic pressure difference across the septal wall. In the reduced version of the model used in this study, ventricular–ventricular interaction along with inertance of the blood moving through the four heart valves is omitted.

Table 2. Equations for calculating nominal parameter values

	Parameter	Units	Equation	Mean ± STD	Reference
Heart Parameters	H	s^{-1}	heart rate	90.66 ± 12.91	
	T	s	H^{-1}	0.33 ± 0.05	
Left ventricle	E_{lv}	mmHg·ml^{-1}	$\frac{P_{sa,syst} - P_{th}}{V_{lv,m} - V_{d,lvf}}$	1.7 ± 0.6	*
	$V_{d,lv}$	ml		10	Williams *et al.* (2014)
	$P_{0,lv}$	mmHg		0.125	**
	λ_{lv}	ml^{-1}		0.029 ± 0.005	**
	$V_{0,lv}$	ml		12	**
Right ventricle	E_{rv}	mmHg·ml^{-1}	$\frac{P_{pa,syst} - P_{th}}{V_{rv,m} - V_{d,rvf}}$	0.44 ± 0.23	*
	$V_{d,rv}$	ml		9	**
	$P_{0,rv}$	mmHg		0.25	**
	λ_{rv}	ml^{-1}		0.024 ± 0.004	**
	$V_{0,rv}$	ml		10.8	**
Pulmonary vasculature	E_{pa}	mmHg·ml^{-1}	$\frac{P_{pa,syst} - P_{th}}{\mathrm{CBV}_{pa}}$	0.32 ± 0.09	*
	E_{pu}	mmHg·ml^{-1}	$\frac{P_{pcw}}{\mathrm{CBV}_{pu}}$	0.019 ± 0.08	*
	R_{pul}	mmHg·s·ml^{-1}	$\frac{P_{pa,syst} - P_{pcw}}{\mathrm{CO}}$	0.16 ± 0.05	Ohm's Law/Data
Systemic vasculature	E_{sa}	mmHg·ml^{-1}	$\frac{P_{sa,syst}}{\mathrm{CBV}_{sa}}$	0.69 ± 0.09	*
	E_{sv}	mmHg·ml^{-1}	$\frac{\frac{1}{3}P_{sv,syst} + \frac{2}{3}P_{sv,diast}}{\mathrm{CBV}_{sv}}$	0.02 ± 0.01	*
	R_{sys}	mmHg·s·ml^{-1}	$\frac{P_{sa,syst} - (\frac{1}{3}P_{sv,syst} + \frac{2}{3}P_{sv,diast})}{\mathrm{CO}}$	1.14 ± 0.25	Ohm's Law/Data
Heart valves	R_{mt}	mmHg·s·ml^{-1}	$\frac{P_{pu,diast} - P_{lv,diast}}{\mathrm{CO}}$	0.0025 ± 0.0009	Ohm's Law/Data
	R_{av}	mmHg·s·ml^{-1}	$\frac{P_{lv,syst} - P_{sa,syst}}{\mathrm{CO}}$	0.029 ± 0.006	Ohm's Law/Data
	R_{tc}	mmHg·s·ml^{-1}	$\frac{P_{sv,diast} - P_{rv,diast}}{\mathrm{CO}}$	0.0011 ± 0.0008	Ohm's Law/Data
	R_{pv}	mmHg·s·ml^{-1}	$\frac{P_{rv,syst} - P_{pa,syst}}{\mathrm{CO}}$	0.028 ± 0.025	Ohm's Law/Data

The total flow through the system equals CO (converted to ml/s), CBV denotes the circulating blood volume, P the blood pressure, and H heart rate (converted to 1/s). Subscripts: *lv* denotes the left ventricle, *rv* the right ventricle, *lvf* the left ventricular free wall, *rvf* the right ventricular free wall, *syst* systole, *diast* diastole, *m* mean, *d* the dead space, *pa* pulmonary arteries, *pu* pulmonary veins, *sa* systemic arteries, and *sv* systemic veins. Entries noted with $*$ are computed by rearranging the model equations and using available data as described in the methods section. Entries noted with $**$ are set by hand fitting normal CV function model output to the Smith model output using values in the CellML version of the Smith model (Nielsens, 2010) as a guide.

$$\mathrm{BSA} = \begin{cases} 0.0005795\ \mathrm{BW}^{0.38}\ \mathrm{Hgt}^{1.24} & \text{for males} \\ 0.0009755\ \mathrm{BW}^{0.46}\ \mathrm{Hgt}^{1.08} & \text{for females.} \end{cases} \quad (11)$$

TBV is used to estimate the volumes in the systemic vasculature while BSA is used to estimate mean left and right ventricular volumes as shown later. Following approximations by Beneken *et al.* (1967) the total blood volume is distributed as 3.5% in the left ventricle, 3.5% in the right ventricle, 3% in the pulmonary arteries, 11% in the pulmonary veins, 13% in the systemic arteries, and 64% in the systemic veins. The compartment models only track stressed volume which we assume are approximately the following for the distributed volumes in each individual compartment: 27% in the systemic arteries, 58% in the pulmonary arteries, 18% in the systemic veins, and 11% in the pulmonary veins.

Pressure

In order to estimate nominal parameter values for elastances and resistances, pressures must be estimated or extracted from the clinical data. EHRs with RHC procedures include measurements of systolic and diastolic pressures in the right ventricle and the main pulmonary artery along with the capillary wedge pressure which effectively represents the mean pressure in the pulmonary veins. In addition, systemic arterial blood pressure is measured using a pressure cuff. Using these values, we can estimate other pressures in the cardiovascular system. First, we estimate the diastolic pressure in the pulmonary veins. For this, we use the capillary wedge pressure which we assume to represent the mean pulmonary venous pressure. We then assume that the pulmonary venous pulse pressure is roughly 20% of the measured pulmonary arterial pulse pressure as based on observations in a

normotensive human study (Caro *et al.* 1967) and then calculate the diastolic pressure as the mean pressure minus 33% of the pulse pressure.

$$P_{pu,pp} = 0.2P_{pa,pp}, \tag{12}$$

$$P_{pu,diast} = P_{pcw} - 0.33P_{pu,pp}. \tag{13}$$

In addition, we need to estimate systolic and diastolic pressures for the left ventricle, and the vena cava. The systolic pressure in the left ventricle is of the same order of magnitude as the systolic arterial pressure and the diastolic pressures in the left ventricle and vena cava are similar to the pulmonary venous diastolic pressures and right ventricular diastolic pressure. Assuming a 2.5% pressure drop across the mitral, aortic and tricuspid valves, we can approximate these three pressures as

$$P_{lv,syst} = 1.025P_{sa,syst,} \tag{14}$$

$$P_{lv,diast} = 0.975P_{pu,diast}, \tag{15}$$

$$P_{sv,diast} = 1.025P_{rv,diast}. \tag{16}$$

Furthermore, we estimate the systolic vena cava pressure assuming that the pulse pressure in the vena cava $P_{sv,pp}$ is 5% of systemic arterial pulse pressure, giving

$$P_{sv,syst} = P_{sv,diast} + P_{sv,pp}. \tag{17}$$

Stroke volume

Using the cardiac output (CO (ml·s^{-1})) and heart rate (H ((1 s^{-1})) data we can calculate the stroke volume, SV (ml), by

$$\mathrm{SV} = \frac{\mathrm{CO}}{H}. \tag{18}$$

Volume

Using a linear regression from Gutgesell & Rembold (1990), we calculate the end-diastolic left ventricular volume as

$$V_{lv} = 93\ \mathrm{BSA} - 16, \tag{19}$$

where BSA denotes the body surface area (in m^2) calculated in eqn (11). From eqns (18) and (19), we calculate the volume of the left ventricle at the end of systole as

$$V_{lv} = V_{lv} - \mathrm{SV}. \tag{20}$$

Accurate measurements of right ventricular volumes are difficult because of the complex geometry of the right ventricular chamber. For the purpose of our nominal parameter calculations we assumed that right ventricular end-diastolic and end-systolic volumes were estimated at roughly 0.9 times the corresponding left ventricular volumes based on observations that the right ventricle chamber volumes are slightly smaller than in the left heart (Hergan *et al.* 2008; Tamborini *et al.* 2010).

Elastance

Nominal elastance parameter values are needed for all compartments. Nominal elastance parameters are calculated by combining information in eqns (2), (5) and (6) with the estimated compartmental blood volume (CBV) in compartment i to give

$$E_i = \frac{P_{i,syst} - P^*_{th}}{CBV_i - V^*_{d,i}}. \tag{21}$$

where i is sa, sv, rv, pa, pu and lv. Equation (21) has three forms. For compartments inside the thorax (pa, pu, rv, lv), the systolic pressure is offset by the intra-thoracic tissue pressure P^*_{th}. This term is not included in calculations predicting elastance in the systemic arteries and veins as these are mostly outside the thorax. Finally, the CBV is offset by $V^*_{d,i}$, a dead space volume, in compartments representing the left and right ventricles.

Resistances

Nominal values of the resistances in each compartment of the model are calculated from the fluid equivalent of Ohm's Law using measured CO as our baseline flow and the estimated or measured pressures for P_{in} and P_{out}

$$R_i = \frac{P_{in} - P_{out}}{\mathrm{CO}}. \tag{22}$$

In 12 sets of RHC data the systolic pulmonary artery pressure was recorded as greater than or equal to the systolic right ventricular pressure. Since this would yield an unrealistic zero or negative resistance, for these patients we set

$$P_{pa,syst} = 0.95P_{rv,syst} \tag{23}$$

to estimate the nominal value of the resistance across the pulmonary valve.

Remaining parameters

The remaining parameters were set to nominal parameter values from the literature or hand-tuned to fit normal cardiovascular function as determined by Smith *et al.* (Table 2). All nominal parameter sets are then checked to make sure the model output is sufficiently close to the RHC measures for a given patient. In a few patients, the

left and right ventricular diastolic relaxation parameters, λ_{lv} and λ_{rv}, are adjusted from the Smith nominal values to more closely represent the RHC measurements before the sensitivity analysis or parameter optimization is performed.

Sensitivity analysis

With unique sets of nominal parameter values determined for each patient RHC we use local sensitivity analysis to determine the relative importance of the parameters in the neighbourhood of the nominal values. Given that both the model output and parameters contain quantities of different orders of magnitude and units, we compute a relative sensitivity matrix S defined by

$$S_{i,j} = \frac{\partial y(t_i, \theta)}{\partial \theta_j} \frac{\theta_j}{y_i^d}, \tag{24}$$

where $y(t_i, \theta)$ represents the model output at time t_i, θ_j denotes the jth parameter, and y_i^d denotes the data measured at time t_i. Due to the complexity of the model, S is difficult to calculate analytically, so similar to Pope *et al.* (2009) we use finite differences to estimate S by

$$S_{i,j} = \frac{y(t_i, \theta + he_j) - y(t_i, \theta)}{h} \frac{\theta_j}{y_i^d}. \tag{25}$$

Here $h = \sqrt{\epsilon}$ where ϵ is the tolerance (set at 10^{-12}) of the ordinary differential equation solver, and e_j is the unit vector in the jth direction. To approximate the influence that each parameter has on the model, we rank the sensitivity for parameter j, R_j, as the two-norm over each column of the relative sensitivity matrix, S

$$R_j = \left(\sum_{i=1}^{N} S_{i,j}^2 \right)^{\frac{1}{2}}. \tag{26}$$

Parameter subset selection

In addition to being sensitive, it is important that estimated parameters are not correlated (Marquis *et al.* 2018). To determine a subset of independent parameters we used sensitivity-based covariance analysis (Olufsen & Ottesen, 2013) to get *a priori* insight into the potential correlation structure. For all sensitive parameters, we calculate the covariance matrix

$$c_{ij} = \frac{C_{ij}}{\sqrt{C_{ii} C_{jj}}}, \quad C = \left(S^T S \right)^{-1}, \tag{27}$$

where S denotes the sensitivity matrix. This formulation is valid under the assumption that the variance is constant. The covariance matric C is defined if $S^T S$ (also known as the Fisher information matrix) can be inverted necessitating the *a priori* removal of parameters that are perfectly correlated. Parameters for which $c_{ij} > \gamma$ (here we let $\gamma = 0.9$) are denoted as correlated. Following the structured correlation method by Ottesen and Olufsen (2013), the covariance matrix is analysed for all sensitive parameters. It is an iterative algorithm that removes the least sensitive parameter from a pair of correlated parameters. Parameters are removed sequentially until an uncorrelated subset is identified. Before the structured analysis discussed above, analytical knowledge is used to identify parameters that appear in structurally correlated combinations. All parameters that are removed from the subset are fixed at their nominal value. This analysis is local in nature as the sensitivity matrix is evaluated at nominal parameter values determined for each patient.

Model optimization and parameter identifiability

Next, we use the cardiovascular system model to reproduce the clinical measures from the RHC procedure along with systemic arterial blood pressure. Clinical measures of patient height, weight and sex are used to estimate the total blood volume (eqn 10) and heart rate is used to drive the model (eqn 1). The remaining measures are matched to the output of the model simulation (light grey shaded measures in Table 1). For each patient, we estimate a subset of parameters θ^*, that minimize the least squares error

$$J = r^T r, \tag{28}$$

where r is the residual vector containing eight entries r_i, $1 \leq i \leq 8$, where

$$r_{1-3} = r_k = \frac{1}{\sqrt{8}} \cdot \frac{\max\left[P_k(\tilde{t})\right] - P_{k,syst}^d}{P_{k,syst}^d}, \; k = \{sa, pa, rv\} \tag{29}$$

$$r_{4-6} = r_k = \frac{1}{\sqrt{8}} \cdot \frac{\min\left[P_k(\tilde{t})\right] - P_{k,diast}^d}{P_{k,diast}^d}, \; k = \{sa, pa, rv\} \tag{30}$$

$$r_7 = \frac{1}{\sqrt{8}} \cdot \frac{\frac{\int_0^T P_{pu}(t_i) dt}{T} - P_{pcw}^d}{P_{pcw}^d}, \tag{31}$$

$$r_8 = \frac{1}{\sqrt{8}} \cdot \frac{\frac{\int_0^T Q(t_i) dt}{T} - \mathrm{CO}^d}{\mathrm{CO}^d}, \tag{32}$$

where quantities with superscript d refer to data. For each term, values are calculated over one cardiac cycle after the system has reached a steady state of pulsatile pressures and flows over $\tilde{t} \in (0, T)$. The capillary wedge pressure (P_{pcw}) and cardiac output (CO) represent average values over the cardiac cycle. Therefore, time-varying quantities Q and P_{pu} are averaged over the stable cardiac cycle before being compared with the data. Given that quantities

minimized are of different units, each residual function is divided by a characteristic value for the quantity. Point estimates for the identifiable parameters are obtained using the Levenberg–Marquardt optimization routine by Kelley (1999) and since parameters vary in magnitude we estimate the log-scaled parameters as outlined in Marquis *et al.* (2018). To ensure convergence we repeated parameter estimation starting with eight initial parameter sets, varying the nominal parameter values by 10%.

To overcome the limitation of the local approach, similar to Marquis *et al.* (2018) we applied the delayed rejection adaptive metropolis (DRAM) (Haario *et al.* 2006; Smith, 2013), a Metropolis–Hastings type Markov chain Monte Carlo (MCMC) algorithm, to verify that our deterministic results are reasonable. MCMC is a widely used sampling method which allows the study of sample point distributions per the evaluation of iteratively generated random samples, each strictly dependent on the previous one. More specifically, DRAM is an acceptance–rejection algorithm accepting, or rejecting, newly generated parameters during each iteration based on their ability to satisfy a higher likelihood than the current evaluated parameter. If a parameter is rejected, delayed rejection permits the further evaluation of other parameters (Smith, 2013).

For this analysis we used a normal joint *a priori* distribution with the mean obtained from the point estimate obtained using the Levenberg–Marquardt gradient-based optimization method (Kelley, 1999). The *a priori* estimates are used as initial values in the DRAM algorithm, in turn calculating a posterior distribution which allows us to study the potential of pairwise correlations and possible impacts on identifiability.

Results

Sensitivity, subset selection and comparison of model predictions

In this study we selected two subsets of parameters to analyse. The first is based on known parameters of physiological interest, whereas the second is formed to include identifiable parameters determined from local sensitivity and structured correlation analysis. Figure 3 presents the normalized ranked parameter sensitivities for a characteristic dataset and the two parameter subsets chosen for this study for patient 233. R_{av} and R_{mt} are not included in the subset as their ranked sensitivities are less than 0.01. These parameters were fixed at their nominal values and not included in correlation analysis. To justify fixing these parameters we doubled and halved them noting that changing their value has a negligible effect on dynamic model predictions. For the remaining parameters, we used the structured correlation algorithm (Olufsen & Ottesen, 2013) to determine an identifiable parameter set. For all patients, we used a correlation threshold of $\gamma = 0.9$. This analysis determined the following sensitivity-based identifiable parameter subset including:

$$\hat{\theta} = \left\{\lambda_{rv},\ \lambda_{lv},\ E_{pa}, E_{pu}, R_{pul}, E_{sa}, R_{sys},\ R_{pv}\right\}.$$

When this analysis was run on other patient data in the study the same identifiable subset emerged, although in some cases the ranking order changed slightly. Results shown in Fig. 4 for patient 233 are obtained by estimating the sensitivity-based identifiable subset $\hat{\theta}$ keeping all other parameters fixed at their nominal value. Results shown in Fig. 4 are obtained by minimizing the least square error as presented in eqn (28). The optimized parameter values $\hat{\theta}_{opt}$ are given in Table 3.

Results for patient 233 are shown in Fig. 5 estimating the physiology-based parameter subset $\tilde{\theta} = \{E_{rv}, E_{lv}, R_{sys}, E_{pu}, R_{pul}, E_{pa}, R_{pv}, E_{sa}, V_{d,lv}\}$. The optimized parameter values for this subset are given in Table 3. Note that the two subsets $\hat{\theta}$ and $\tilde{\theta}$ have six parameters in common, $\theta_{com} = \{R_{sys}, E_{pu}, R_{pul}, E_{pa}, R_{pv}, E_{sa}\}$. From a physiological point of view, the systolic elastances of the left and right ventricles (E_{lv} and E_{rv}) are easier to interpret than the parameters defining diastolic filling (λ_{lv} and λ_{rv}),

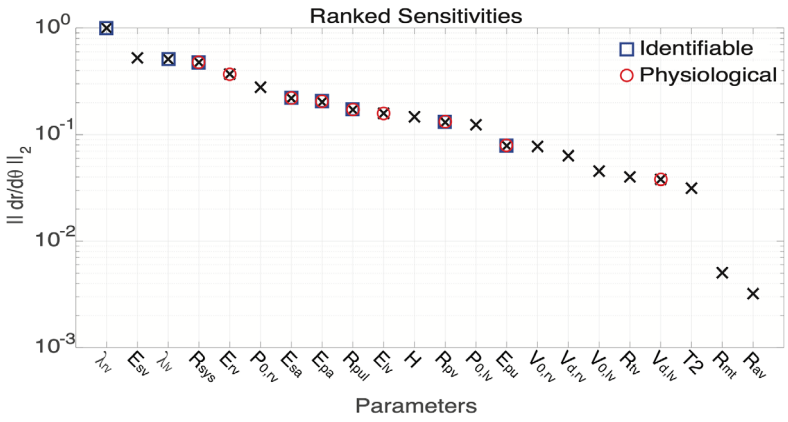

Figure 3. Ranked sensitivities for patient 233
Blue squares indicate the parameters selected by identifiability after sensitive parameters were also assessed for structural correlation while the red circles indicate those thought to be interesting based on their physiological meaning. Rank sensitivities for other patients in this study produces very similar rankings and yielded the same identifiable parameter subset.

and therefore are included in the physiological subset $\tilde{\theta}$. However, correlation analysis revealed that parameters E_{rv} and λ_{rv} in addition to E_{lv} and λ_{lv} are correlated and that the elastance parameters are less sensitive. Therefore, the identifiable parameter set $\hat{\theta}$ includes λ_{lv}, λ_{rv} and fixes E_{lv} and E_{rv} at their nominal values. Next, we observe that $V_{d,lv}$ is strongly correlated with E_{rv}, E_{lv}, R_{sys}, E_{pu} and E_{sa}. Removing $V_{d,lv}$ from the subset, fixing it at its nominal value, eliminated correlations within the remaining subset.

When we optimize $\hat{\theta}$ and $\tilde{\theta}$, the residual least squares cost are both small (e.g. 1.5×10^{-5} and 1.67×10^{-3}, respectively, for patient 233) but the residual is smaller with the sensitivity-based identifiable parameter subset. In addition, the physiology-based parameter subset, $\tilde{\theta}$, for patient 233 gives estimations of left and right ventricular volume that differ significantly in magnitude (Fig. 5*F*) while in the sensitivity-based identifiable parameter subset, $\hat{\theta}$, of the optimized model the systolic and diastolic volumes for the ventricles are similar in magnitude (Fig. 4*F*). Systolic and diastolic volumes for the right and left ventricles are expected to be similar in a normal cardiovascular state (Alfakih *et al.* 2003), which is in line with the sensitivity-based identifiable parameter subset optimization predictions; however, no studies have been performed that quantify relative ventricular volumes in post-transplant hearts.

Table 3. Nominal and optimized parameter values for patient 233 using the sensitivity-based identifiable parameter subset, $\hat{\theta}$ and the physiology-based parameter subset, $\tilde{\theta}$

			Optimized	
Parameter	Units	Nominal	SBIP, $\hat{\theta}$	PBP, $\tilde{\theta}$
λ_{lv}	ml	0.03	0.0289	—
λ_{rv}	ml^{-1}	0.025	0.0183	—
E_{lv}	$mmHg \cdot ml^{-1}$	3.51	—	2.704
$V_{d,lv}$	ml	10	—	8.13
E_{rv}	$mmHg \cdot ml^{-1}$	0.92	—	3.65
E_{pa}	$mmHg \cdot ml^{-1}$	0.39	0.1696	0.2074
E_{pu}	$mmHg \cdot ml^{-1}$	0.30	0.212	0.1059
R_{pul}	$mmHg \cdot s \cdot ml^{-1}$	0.095	0.0481	0.05015
E_{sa}	$mmHg \cdot ml^{-1}$	0.820	0.678	0.767
R_{sys}	$mmHg \cdot s \cdot ml^{-1}$	0.835	0.637	0.715
R_{pv}	$mmHg \cdot s \cdot ml^{-1}$	0.029	0.00797	0.00777

Parameter definitions: λ, ventricular end-diastolic pressure-volume exponent, E, elastance, and R, resistance. Subscripts: *lv*, left ventricle, *rv*, right ventricle, *pa*, pulmonary artery, *pu*, pulmonary veins, *pul*, pulmonary circulation, *sa*, systemic arteries, *sys*, systemic circulation, *pv*, pulmonary valve.

Parameter identifiability

We performed a DRAM analysis to confirm the degree of identifiability for each of our two parameter subsets and to further uncover which parameters in the subset

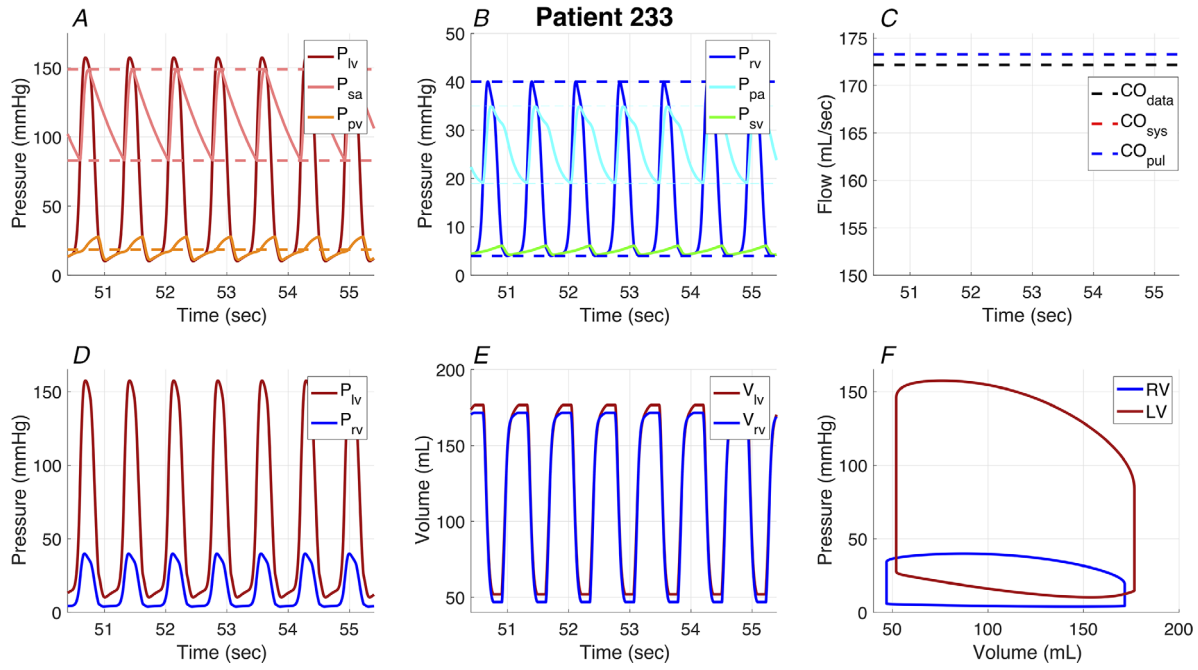

Figure 4. Model predictions for subject 233 with optimized sensitivity-based identifiable parameters, $\hat{\theta}$
Left ventricle, pulmonary vein and systemic arterial pressure (*A*) and right ventricle, pulmonary artery and systemic venous pressure (*B*) comparison of computed results (continuous lines) and data (broken lines). *C*, comparison of computed cardiac output and data. *D*, comparison of left and right ventricular pressure. *E*, computed left and right ventricular volume (no data available). *F*, left and right ventricular pressure-volume loops.

are correlated. For each of the two parameter subsets $\hat{\theta}$ and $\tilde{\theta}$ we set up a normal joint *a priori* distribution with the mean obtained from the point estimates discussed above. The DRAM algorithm was run with 100,000 sample points. To ensure that our solutions converge to a steady state prior to calculating the posterior distributions and correlations we removed, the burn-in period was set to 10,000 sample points. Figure 6 shows that for both parameter subsets, the chains have converged (top two panels). The bottom panels in Fig. 6 show the posterior distributions for each parameter in both subsets. For the physiological subset $\tilde{\theta}$, we observed that the parameter $V_{d,lv}$, for the dead space volume in the left ventricle, has an identical distribution to the parameter E_{lv}, the elastance of the left ventricle. This distribution suggests that the parameters are correlated with a single valued relationship; this is equivalent to saying their Pearson correlation is +1. A Pearson correlation of +1 is indicative of a perfect positive linear relationship (Everitt & Skrondal, 2010) between the parameters which is confirmed in Fig. 7 depicting pairwise distributions. Therefore, fixing one of the two parameters may improve the DRAM results of the physiology-based parameter subset since they are not mutually identifiable. Additionally, posterior and pairwise distributions for the sensitivity-based identifiable parameter subset confirm local observations that all parameters are independent.

Longitudinal analysis

Using the cardiovascular system model with the sensitivity-based identifiable parameter subset, RHC measurements were analysed to represent cardiovascular functional changes during recovery in five of the 10 patients where multiple RHC measurements were available. Figure 8 shows the changes in cardiovascular function, as indicated from simulated left and right ventricular PV loops and left and right ventricular power output, for two representative patients (patients 266 and 558). Ventricular power output can be calculated by integrating the area inside the PV loop and multiplying it by heart rate. The adoption of left ventricular power as a clinical measure is becoming more common (Cotter *et al.* 2003*b*; Fincke *et al.* 2004) and has been shown to be elevated at rest in septic shock and congestive heart failure with hypertension (Cotter *et al.* 2003*a*). Figure 8 shows a consistent reduction in right and left ventricular pressure as well as left and right ventricular

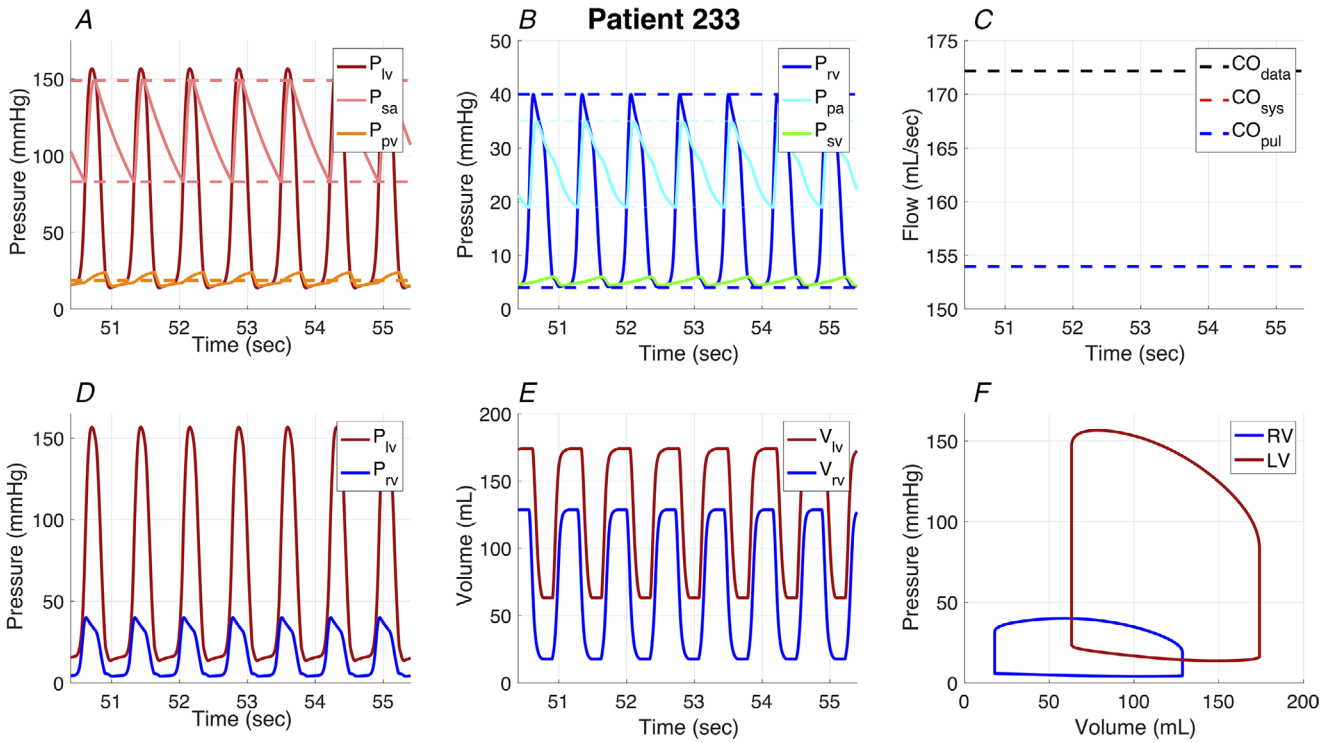

Figure 5. Model predictions for subject 233 with optimized physiology-based parameters, $\tilde{\theta}$
Left ventricle, pulmonary vein and systemic arterial pressure (*A*) and right ventricle, pulmonary artery and systemic venous pressure (*B*) comparison of computed results (continuous lines) and data (broken lines). *C*, comparison of computed cardiac output and data. *D*, comparison of left and right ventricular pressure. *E*, computed left and right ventricular volume (no data available). *F*, left and right ventricular pressure-volume loops.

power output during recovery in patient 266 that are not seen with patient 558. For patient 266, the systolic volumes in both ventricles increases during recovery with diastolic volumes remaining relatively constant. However for patient 558, systolic volumes in both ventricles show a great degree of variability with a general reduction during recovery and a left ventricular diastolic volume that remains nearly constant. This representation of cardiovascular function cannot be obtained from the RHC measurements without the use of this computational analysis approach. As shown in Fig. 9, we can also track individual parameters longitudinally; the values of the sensitivity-based identifiable parameter subset are plotted for patients 266 and 558. The remaining three patients with longitudinal RHCs during recovery (363, 456 and 572, not shown) showed small increases in left ventricular cardiac power during recovery of 6, 27 and 22% rising to 1.15, 1.42 and 1.73 W, respectively. All of these values are well below the peak left ventricular power of 2.5 W for patient 558, indicating that left ventricular cardiac power below 2 W during recovery is favourable.

Discussion

In this study, we develop an analysis methodology where a series of RHC measurements from recovering heart transplant patients are analysed with an identifiable model of cardiovascular system dynamics to represent cardiovascular function progression during recovery. In the first portion of this study we carefully assessed which model parameters could be reliably identified with the sparse clinical data from EHRs including RHC measurements, systemic arterial blood pressure, heart rate, and other biometrics from the patient. A sensitivity-based parameter subset was selected and compared with an alternative parameter subset to show differences in parameter identifiability and correlation. The sensitivity-based parameter subset was shown to be identifiable and composed of independent parameters in the neighbourhood of parameter values optimized to fit clinical data for one exemplary RHC dataset. In the second portion of this study we used this model to analyse recovery progression for five patients that had a series of RHCs over the span of 7 to 392 days post-transplant. Trends

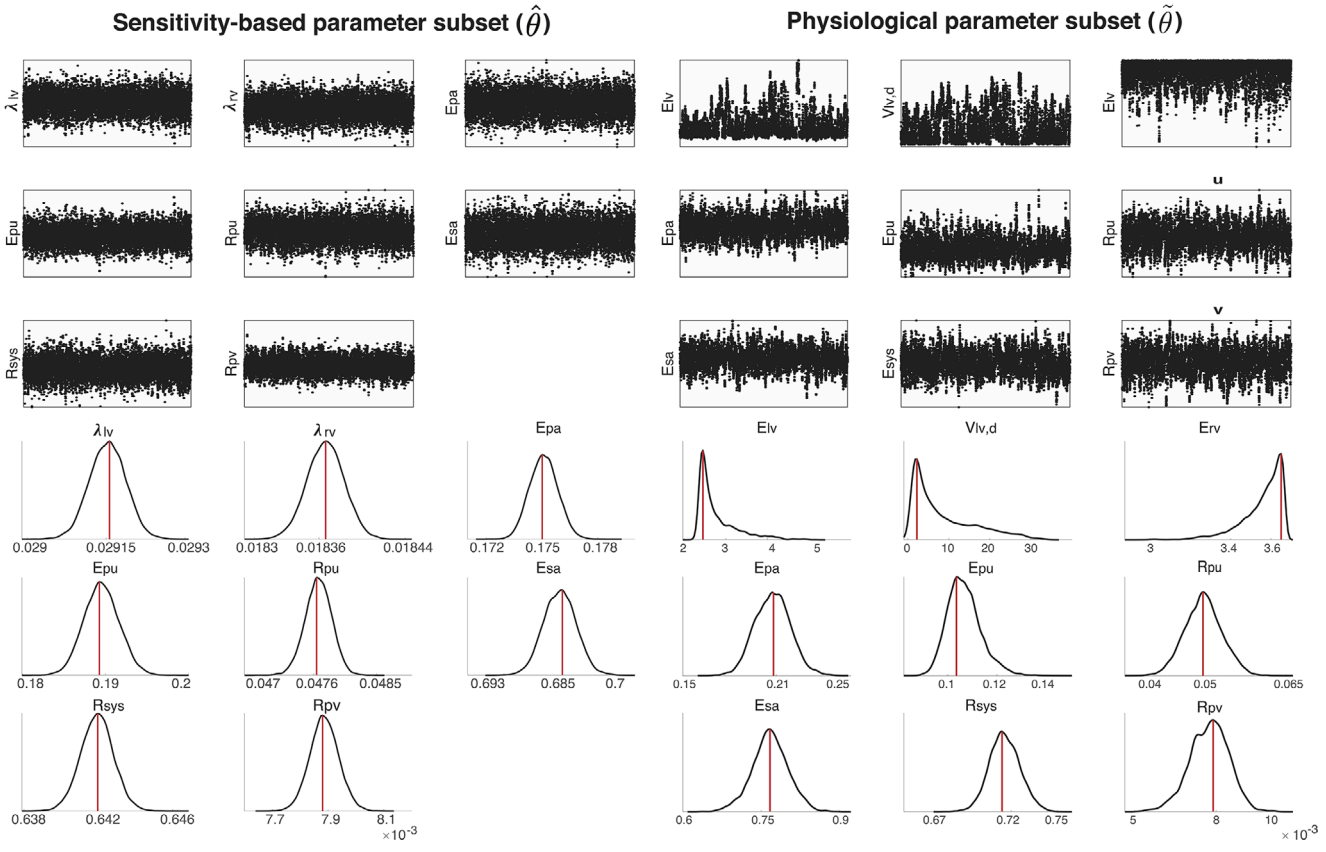

Figure 6. Convergence chains and posterior distributions for inferred parameters
DRAM-based convergence chains (upper two panels) and parameter distributions (lower two panels) at optimized parameter values for patient 233 using the sensitivity-based identifiable (left column panels) and physiology-based (right column panels) parameter subsets. Note that the parameter distributions for the sensitivity-based parameter subset are narrower than seen in the physiology-based subset for all common parameters.

in simulated PV loops, left and right ventricular power output and model parameters over the course of recovery show differences in recovery progression. Two patients (266 and 558) were selected from the analysis that show distinct differences in recovery.

Longitudinal analysis of cardiovascular function

It is known that pulmonary hypertension (>25–30 mmHg) is often observed post-transplant with a trend to normal right-side pressures (∼20 mmHg) in a successful recovery (Delgado *et al.* 2001). We have analysed RHC datasets at several post-transplant time points in patients 266, 363, 456, 558 and 572 to see what other cardiovascular metrics may be useful to predict outcome. We focused on patient 266 to represent what appears to be a successful heart transplant recovery.

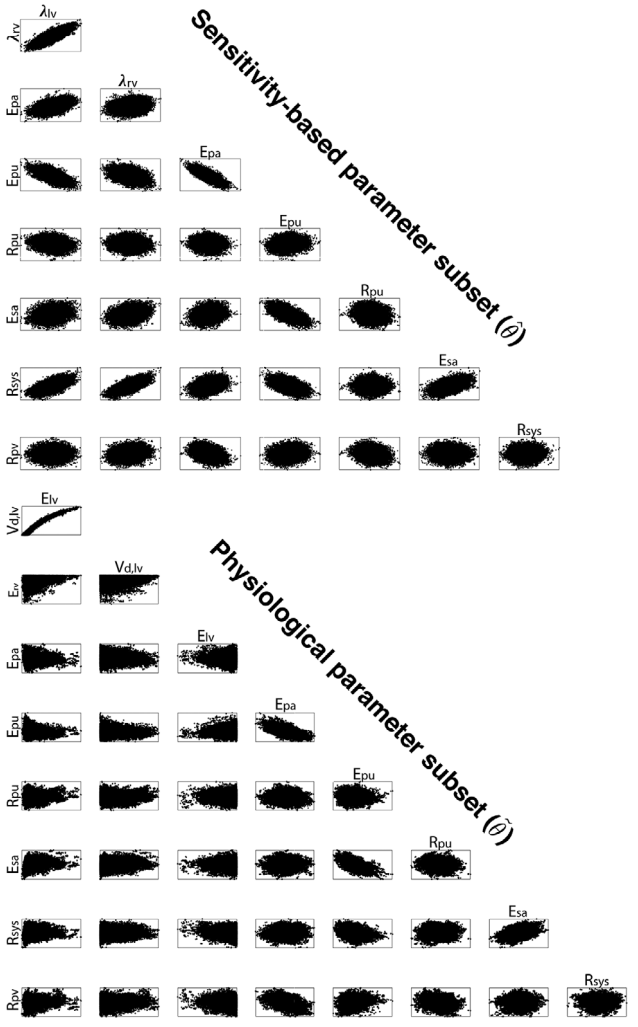

Figure 7. Pairwise posterior distributions for each parameter subset
In the physiology-based parameter subset, E_{lv} and $V_{lv,d}$ are seen to be correlated since the relationship between the two distributions can clearly be seen. Pairwise parameters showing no correlation form a large cloud of points indicating no distinct relationship exists between the two distributions.

For patient 266, left and right PV loop trends as a function of recovery time represented in Fig. 8 show a reduction in right ventricular pressure along with an increase in end-systolic volume over seven time points spanning an 11-month period post-transplant. The RHC data alone show this reduction in ventricular pressures. However, we observe that over time, the ejection fraction decreases by 5%, the left ventricular end-diastolic pressure decreases from about 10 to 6 mmHg, the systemic arterial elastance decreases (reduction in stiffness) by 54% and the systemic resistance decreases by 17%. Even more interesting is the trend in left and right ventricular power output. As recovery progresses, patient 266 experienced a decrease in left ventricular power output from 1.8 W at day 57 post-transplant to 1.4 W at day 392. These predicted metrics describe the constellation of concurrent changes that can be quantified in the transplanted heart, but also account for changes in the pulmonary and systemic cardiovascular system over time. A decreasing trend in ventricular power can be interpreted as the heart working less to maintain cardiac output as the patient recovers. A normal left ventricular power output at rest is around 1 W (Cotter *et al.* 2003*b*; Klasnja *et al.* 2013) and roughly represents a blood pressure of 120/80 mmHg, a heart rate of 70 beats/min and a stroke volume of 70 ml. While the predicted reduction in ejection fraction points to reduced cardiovascular function in this patient, this is likely due to the fact that volumes are not constrained by any clinical measures in this study. The inclusion of periodic echocardiograms along with the heart rate close to the time of each RHC could be used as another set of measurements to bound the left ventricular end-diastolic and end-systolic volumes in the optimized models.

Patient 558, on the other hand, shows a slight increase in right ventricular pressure over the seven time points spanning 5 months. For this patient, the model predicts a consistent left ventricular end-diastolic pressure of about 11 mmHg, a decrease in systemic arterial elastance of 28%, a large increase in systemic resistance of 80% as well as distinct arterial hypertension rising to 180 mmHg as shown in the left ventricular pressure model output. Markedly, the left ventricular power does not show any downward trend and remains high over the observed recovery period, varying between 1.5 and 2.5 W. The predicted increase in systemic resistance for patient 558 is slightly below the range of 120% and 250% increase from normal healthy values of systemic resistance observed in patients with congestive heart failure with hypertension and pulmonary oedema, respectively (Cotter *et al.* 2003*a*) but still reflects a negative trend during recovery. It may also be noted that our computation of cardiac power from generated PV loops takes into account the diastolic

filling pressure, which is ignored in clinical calculations, making this prediction of cardiac power a better estimate in the case of pulmonary hypertension and congestive heart failure when diastolic filling pressures increase. A comparison of cardiovascular metrics between patients 266 and 558 suggests a less successful recovery for patient 558.

To test whether these retrospective predictions align with the actual patient outcome, the EHRs for each of the longitudinally tracked patients were checked in March

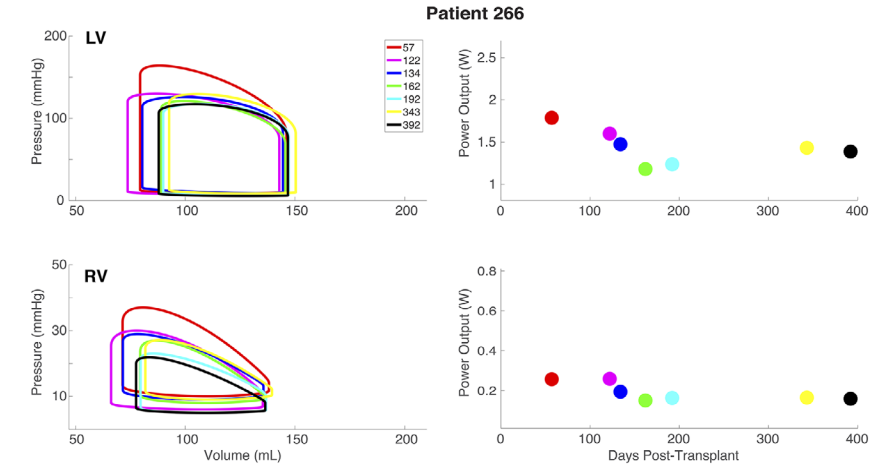

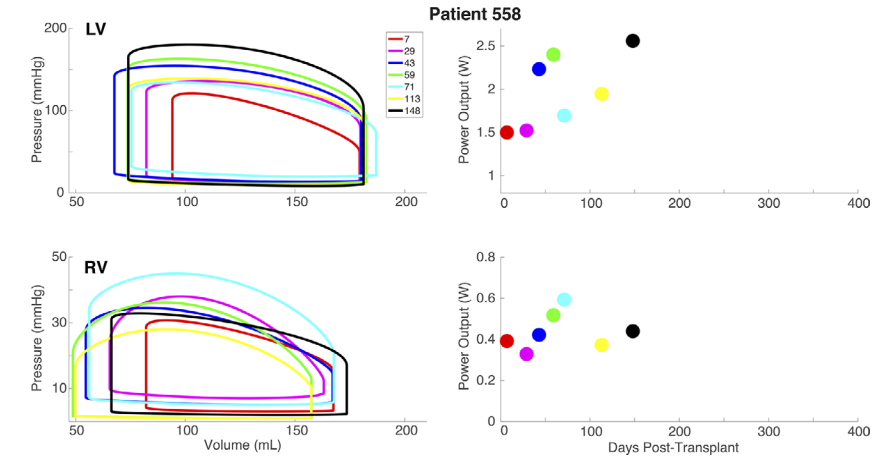

Figure 8. Simulated pressure-volume loops as well as left and right ventricular power output over time for patients 266 and 558
Chronological progression earliest to latest by colour is magenta, red, yellow, green, aqua, blue and black. Even if the EHR contains echocardiography and right heart catheterization (RHC) data, the pressures from RHC and volumes from echocardiography are not obtained simultaneously; therefore, these pressure-volume loops cannot be generated except through a simulation as proposed here. Simulation results for patient 266 and 558 predict dramatically different progression during recovery.

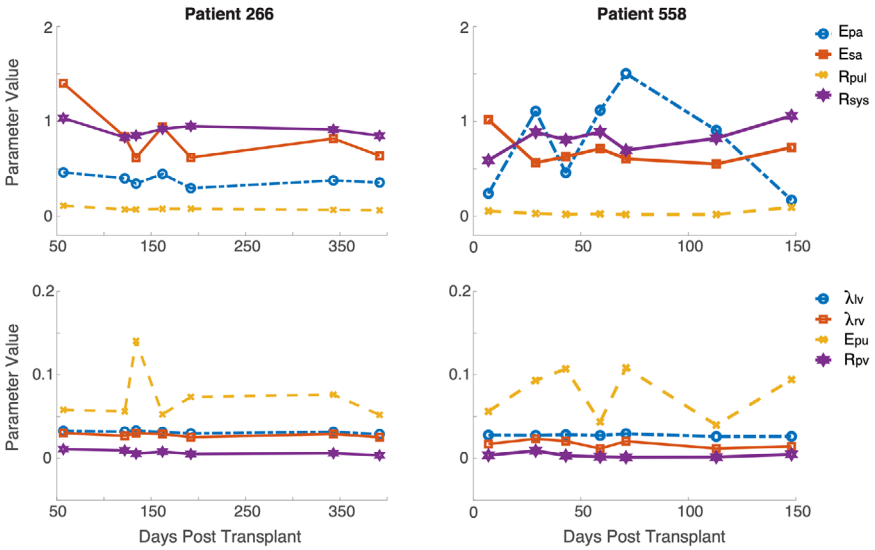

Figure 9. Longitudinal parameter trends for patients 266 and 558
Simulation results are displayed with optimized parameters for the sensitivity-based identifiable parameter subset for patients 266 and 558. Top panels: blue, pulmonary artery elastance, red, systemic arterial elastance, gold, pulmonary circulation resistance, purple, systemic circulation resistance. Bottom panels: blue, left ventricular end diastolic pressure-volume exponent, red, right ventricular end diastolic pressure-volume exponent, gold, pulmonary venous elastance, purple, pulmonary valve resistance

of 2019. This represented post-transplant time points of 54 and 49 months for patients 266 and 558, respectively. Patient 266 exhibited complications due to osteoarthritis, likely precipitated from long-term immunosuppression but had no cardiovascular-related complications. Cardiovascular function checked 43 months post-transplant showed normal cardiovascular function with an ejection fraction at 60% and a stroke volume of 54 ml. In contrast, patient 558 at the 48-month post-transplant time point exhibited biventricular failure with an ejection fraction at 49%, right atrial pressure at 25 mmHg, pulmonary hypertension with right ventricular pressures of 48/35 mmHg, systemic hypertension at 124/98 mmHg, a heart rate of 123 beats/min and diminished stroke volume of 23 ml. The remaining longitudinally tracked patients (363, 456 and 572) predicted to have a positive outcome had no cardiovascular complications noted in their EHRs at post-transplant time points of 47, 46 and 52 months, respectively. Even though the small number of patients tracked in this study does not yet validate this approach, it does illustrate the utility of mechanistic computational analysis of clinical data as a tool for clinicians to use as heart transplant patient recovery is assessed.

Model parameter subset selection

The model selected for this study was developed to estimate the systolic and diastolic pressures, average pulmonary capillary wedge pressure and cardiac output obtained from EHR records. Using the Smith *et al.* (2004) cardiovascular system model as a reference, we carefully selected only the model components that could be informed by the available data. The major components omitted were VVI and inertance at each of the heart valves. A more complex cardiovascular system model could be implemented per the availability of pressure time courses from the RHC measurements and/or the addition of echocardiography data measuring volumes in the left ventricle.

This study compared two parameter subsets. The first was selected based on knowledge of the cardiovascular system and quantities of interest; the second was selected using sensitivity analysis and subset selection. The majority of parameters were present in both subsets, yet rigorous analysis revealed that the physiology-based subset included correlated parameters. The physiology-based parameter subset included resistances of the systemic vasculature (R_{sys}), pulmonary vasculature (R_{pul}) and pulmonary valve (R_{pv}) along with elastances of the left ventricle (E_{lv}), right ventricle (E_{rv}), pulmonary vein (E_{pu}), pulmonary artery (E_{pa}), systemic arteries (E_{sa}) and the dead space volume in the left ventricle ($V_{d,lv}$) as shown by the red squares in Fig. 3. The sensitivity-based subset selection approach omitted $V_{d,lv}$, while identifying the correlation between the elastance parameters in the left and right ventricles and the more sensitive diastolic filling exponents in the left and right ventricle, λ_{lv} and λ_{rv} as shown by the blue circles in Fig. 3. This result suggests that quantifying the parameters determining diastolic filling in the left and right ventricle will have more ability to discriminate underlying cardiovascular function than quantifying the parameters determining systolic contraction. The sensitivity-based approach did not identify the pulmonary valve resistance (R_{pv}) as having high sensitivity. However, this parameter was added to the sensitivity-based identifiable subset since we had data for right ventricular and pulmonary arterial pressure across the valve along with cardiac output. While it is possible to uniquely identify this parameter solely from data, it was included as an adjustable parameter to provide maximum flexibility in matching the two pressures and cardiac output simultaneously.

The physiology-based approach for selecting model parameters to optimize relies on intuition to determine adjustable parameters of interest. However, this approach does not reveal correlations between model parameters, and therefore can lead to subsets which are not uniquely identifiable given the model and associated experimental data. The sensitivity-based approach selected a subset with eight parameters, six of which were also included in the physiology-based parameter subset. In addition to parameter estimation, the sensitivity analysis and subset selection methods employed here can also be used for experimental design, e.g. to analyse what output quantities are needed to estimate specific parameters. The model studied here was simplified compared with the model by Smith *et al.* and a major factor ignored was VVI. This component is believed to be important for patients with severe pulmonary hypertension. However, with clinical measurements only from the right ventricle used in this study, incorporating VVI with the Smith *et al.* model components would likely lead to insensitive parameters in that component of the model.

Finally, it should be noted that in this study the two subsets were studied independently, i.e. the sensitivity-based analysis was purely informed by model analysis. Another approach is to pick parameters of interest and then test whether the subset picked contains identifiable parameters. Finally, the local estimates can be validated by seeing if the point estimates determined using the gradient-based method agree with the maximums of the distributions obtained using DRAM. For this study, this procedure was used for one dataset (patient 233) and the results agreed. Yet both the point estimates and the parameter distributions were obtained subject to values of non-estimated parameters. In future studies, more work is needed to determine the uncertainty to perturbation of fixed parameters within physiological bounds. This can be done using global sensitivity analysis combined

Table 4. Optimized parameter values for first post-transplant right heart catheterization dataset from each patient using the sensitivity-based identifiable parameter subset ($\hat{\theta}$)

		Patient number									
Parameter	Units	60	66	233	266	363	456	558	572	794	839
λ_{lv}	ml^{-1}	0.0353	0.02046	0.0289	0.0328	0.0336	0.0329	0.0277	0.0290	0.0448	0.0283
λ_{rv}	ml^{-1}	0.0185	0.00882	0.0183	0.0303	0.0289	0.0217	0.017	0.0223	0.0316	0.0115
E_{pa}	mmHg $\cdot ml^{-1}$	0.427	0.176	0.1696	0.463	0.243	0.6064	0.2405	0.4603	0.349	0.194
E_{pu}	mmHg $\cdot ml^{-1}$	0.0811	0.0215	0.212	0.0581	0.157	0.0748	0.0562	0.0492	0.40062	0.0289
R_{pul}	mmHg·s·ml^{-1}	0.0471	0.08084	0.0481	0.113	0.147	0.0915	0.0558	0.0653	0.0472	0.0538
E_{sa}	mmHg·ml^{-1}	0.719	0.7105	0.678	1.4007	0.838	0.757	1.018	0.995	0.625	0.9546
R_{sys}	mmHg·s·ml^{-1}	0.975	0.8069	0.637	1.035	1.047	0.878	0.591	0.788	0.6034	1.058
R_{pv}	mmHg·s·ml^{-1}	0.00435	0.00428	0.00797	0.01085	0.0064	0.026	0.00361	0.00562	0.00657	0.01602

Parameter definitions: λ, ventricular end-diastolic pressure-volume exponent, E, elastance, and R, resistance. Subscripts: *lv*, left ventricle, *rv*, right ventricle, *pa*, pulmonary artery, *pu*, plumonary veins, *pul*, pulmonary circulation, *sa*, systemic arteries, *sys*, systemic circulation, *pv*, pulmonary valve.

with more simulations varying these fixed parameters to more completely understand how this variation impacts outcomes.

Model optimization using both selected parameter subsets

Model optimization using both the sensitivity-based and the physiology-based parameter subsets was able to fit the RHC data and systemic arterial pressure measurements, as can be seen by comparing the RHC measurements (dashed lines) and simulated pressure and cardiac output time courses (continuous lines) in panels *A*, *B* and *C* of Figs 4 and 5, respectively. The main differences between the two subsets are in their predictions of the left and right ventricular volume. The physiology-based subset predicts smaller right ventricular volumes and larger left ventricular volumes than the sensitivity-based subset as seen in Figs 4*E, F* and 5*E, F*. The model predictions obtained using the sensitivity-based parameter subset leads to predicted left and right ventricular volumes that are closely matched. It has been observed in normal hearts that the ventricular volumes are typically similar between the right and left sides of the heart (Alfakih *et al.* 2003; Hudsmith *et al.* 2005; Hergan *et al.* 2008), with the right ventricular volume in the order of 5–10% smaller than the left ventricular volume. However, in these same studies right ventricular volumes can be as much as 48% smaller or 68% larger depending on the sex considered, the measurement modality and the method used to calculate the volume from the images obtained. No similar studies have been conducted for ventricular volumes in patients with cardiac hypertrophy, pulmonary hypertension or after heart transplantation.

Confidence in the use of the sensitivity-based identifiable parameter subset is further bolstered by the results of the DRAM analysis as shown in Fig. 6. In the neighbourhood of the model optimization of patient 233 data, parameter distributions for all parameters in the selected sensitivity-based identifiable subset show a narrow Gaussian distribution, whereas the parameter distributions for two parameters in the physiology-based parameter subset, the pairwise distributions for E_{lv} and $V_{d,lv}$ are clearly correlated and their distributions are proportional over the range of each parameter value.

Optimized parameter relationship to cardiovascular function and subsequent model predictions

Optimization of selected model parameters tells us about the underlying function that represents the upper-level phenotype quantified clinically, in this case, with RHC and systemic arterial blood pressure measurements. The optimized model parameters of the first complete RHC dataset from the 10 patients in this study are shown in Table 4; we observe that the five patients (66, 233, 558, 572 and 839) with values for λ_{lv} below 0.03 have the greatest left ventricle diastolic filling. Comparing these patients with the remaining five patients we see mean left ventricular end-diastolic volumes of 178 $\pm$ 23 ml versus 141 $\pm$ 23 ml indicating a strong relationship between λ_{lv} and left ventricular end-diastolic volume.

Since this model is non-linear, it does not encode a one-to-one relationship between each model parameter and the upper-level clinical measurements. However, the power of this approach is that with a model tailored to describe an individual patient's cardiovascular system function, we can make predictions of cardiovascular system function that are not easily measured. One example is the left and right ventricular PV loops, which are often used to more accurately determine functional metrics when available in the clinic. These metrics include the left ventricular end-diastolic and end-systolic pressure-volume relationships and both right and left

ventricular work and power, which show important changes from health to dysfunction. Even though these are important diagnostic metrics, simultaneous measurement of left ventricular volume and pressure without using an invasive indwelling catheter in the left heart is impossible in the clinic; therefore they are rarely obtained. Employing our model analysis with the minimally invasive RHC measurements enables us to predict both right and left ventricular volumes while fitting the cardiovascular pressures in a patient-specific manner, resulting in these PV loops. In Figures 4*D*, *E* and *F* we see the predicted left and right ventricular pressure, volumes and PV loops for patient 233. The relatively high left ventricular diastolic filling pressure shown, resulting from the pulmonary hypertension of the right side along with arterial systemic hypertension warrants close monitoring. However, the left ventricular ejection fraction of about 71% indicates an efficiently functioning heart.

Conclusion

In this study, we have presented a workflow pushing model design and sensitivity analysis prior to model optimization in order to aid in selecting the model parameters that are most likely to be informed by the clinical measurements. We have used clinical RHC and systemic arterial blood pressure data taken from patients shortly after heart transplantation, to determine an identifiable parameter subset, and contrasted it with a subset that was selected based on physiological features of interest. Optimization of both parameter subsets replicated the clinical data equivalently. However, a single insensitive parameter in the physiology-based subset decreased the confidence in the identification of the remaining parameters and the predictions made by the physiology-based subset of the optimized model. To illustrate the potential to track cardiovascular function over time, model optimizations were performed on multiple RHC and systemic arterial pressure measurements for several patients and the trends in model parameters were shown. Predictions made by looking at model results based on these retrospective longitudinal data were confirmed by following up on these patients at the 4-year post-transplant time point illustrating the utility of this patient-specific model analysis. This approach has the ability to provide clinicians with previously unobtainable functional information, such as left and right ventricular PV loops and systemic vascular resistance, from routinely obtained RHC measures. This additional functional information is not only valuable in the assessment of post-heart transplant recovery, but in other cases of cardiovascular dysfunction where RHC measurements are made such as heart failure both with reduced and preserved ejection fraction or pulmonary hypertension.

Appendix: Model equations

The complete list of differential equations representing the rate of change of volume of the compartments in this study are as follows:

$$\frac{dV_{lv}}{dt} = Q_{mt} - Q_{av}$$

$$\frac{dV_{sa}}{dt} = Q_{av} - \frac{E_{sa}V_{sa} - E_{sv}V_{sv}}{R_{sys}}$$

$$\frac{dV_{vc}}{dt} = \frac{E_{sa}V_{sa} - E_{sv}V_{sv}}{R_{sys}} - Q_{tc}$$

$$\frac{dV_{rv}}{dt} = Q_{tc} - Q_{pv}$$

$$\frac{dV_{pa}}{dt} = Q_{pv} - \frac{E_{pa}V_{pa} - E_{pu}V_{pu}}{R_{pul}}$$

$$\frac{dV_{pu}}{dt} = \frac{E_{pa}V_{pa} - E_{pu}V_{pu}}{R_{pul}} - Q_{mt}$$

where

$$Q_{mt} = \begin{cases} \frac{(E_{pu}V_{pu}+P_{th})-P_{lv}}{R_{mt}} & \text{if valve open } (P_{pu} > P_{lv}) \\ 0 & \text{otherwise (valve closed)} \end{cases}$$

$$Q_{av} = \begin{cases} \frac{P_{lv}-E_{sa}V_{sa}}{R_{av}} & \text{if valve open } (P_{lv} > P_{sa}) \\ 0 & \text{otherwise (valve closed)} \end{cases}$$

$$Q_{tc} = \begin{cases} \frac{E_{sv}V_{sv}-P_{rv}}{R_{tc}} & \text{if valve open } (P_{sv} > P_{rv}) \\ 0 & \text{otherwise (valve closed)} \end{cases}$$

$$Q_{pv} = \begin{cases} \frac{P_{rv}-(E_{pa}V_{pa}+P_{th})}{R_{pv}} & \text{if valve open } (P_{rv} > P_{pa}) \\ 0 & \text{otherwise (valve closed)} \end{cases}$$

and

$$P_{lv} = A(\tilde{t})\left[E_{lv}\left(V_{lv} - V_{d,lv}\right)\right] + \left\{\left[1 - A(\tilde{t})\right]P_{0,lv}\left[e^{\lambda_{lv}(V_{lv}-V_{0.lv})} - 1\right]\right\} + P_{th}$$

$$P_{rv} = A(\tilde{t})\left[E_{rv}\left(V_{rv} - V_{d,rv}\right)\right] + \left\{\left[1 - A(\tilde{t})\right]P_{0,rv}\left[e^{\lambda_{rv}(V_{rv}-V_{0.rv})} - 1\right]\right\} + P_{th}$$

$$A(\tilde{t}) = e^{-a(\tilde{t}-T/2)^2}$$

References

Alfakih K, Plein S, Thiele H, Jones T, Ridgway JP & Sivananthan MU (2003). Normal human left and right ventricular dimensions for MRI as assessed by turbo gradient echo and steady-state free precession imaging sequences. *J Magn Reson Imaging* **17**, 323–329.

Armitage JM, Hardesty RL & Griffith BP (1987). Prostaglandin E_1: an effective Treatment of right heart failure after orthotopic heart transplantation. *J Heart Transplant* **6**, 348–351.

Beard DA, Pettersen KH, Carlson BE, Omholt SW & Bugenhagen SM (2013). A computational analysis of the long-term regulation of arterial pressure. *F1000Research* **2**, 208.

Bhatia SJS, Kirshenbaum JM, Shemin RJ, Cohn LH, Collins JJ, Disesa VJ, Young PJ, Mudge GH & Sutton MGS (1987). Time course of resolution of pulmonary hypertension and right ventricular remodeling after orthotopic cardiac transplantation. *Circulation* **76**, 819–826.

Beneken JEW (1967). A physical approach to hemodynamic aspects of the human cardiovascular system. *Physical bases of circulatory transport: regulation and exchange*. W.B. Saunders, Philadelphia, PA, USA.

Caro CG, Harrison GK & Mognoni P (1967). Pressure wave transmission in the human pulmonary circulation. *Cardiovasc Res* **1**, 91–100.

Cotter G, Moshkovitz Y, Kaluski E, Milo O, Nobikov Y, Schneeweiss A, Krakover R & Vered Z (2003*a*). The role of cardiac power and systemic vascular resistance in the pathophysiology and diagnosis of patients with acute congestive heart failure. *Eur J Heart Fail* **5**, 443–451.

Cotter G, Williams SG, Vered Z & Tan LB (2003*b*). Role of cardiac power in heart failure. *Curr Opin Cardiol* **18**, 215–222.

Dandel M, Hummel M, Muller J, Wellnhofer E, Meyer R, Solowjowa N, Ewert R & Hetzer R (2001). Reliability of tissue Doppler wall motion monitoring after heart transplantation for replacement of invasive routine screenings by optimally timed cardiac biopsies and catheterizations. *Circulation* **104**, I184–I191.

Delgado JF, Gomez-Sanchez MA, de la Calzada CS, Sanchez V, Escribano P, Hernandez-Afonso J, Tello R, de la Camara AG, Rodriguez E & Rufilanchas JJ (2001). Impact of mild pulmonary hypertension on mortality and pulmonary artery pressure profile after heart transplantation. *J Heart Lung Transpl* **20**, 942–948.

Du Bois D & Du Bois EF (1916). A formula to estimate the approximate surface area if height and weight be known. *Arch Intern Med* **17**, 863–871.

Everitt BS & Skrondal A (2010). *The Cambridge Dictionary of Statistics*. Cambridge University Press, Cambridge, U.K.

Fincke R, Hochman JS, Lowe AM, Menon V, Slater JN, Webb JG, LeJemtel TH, Cotter G & Invest TS (2004). Cardiac power is the strongest hemodynamic correlate of mortality in cardiogenic shock: A report from the SHOCK trial registry. *J Am Coll Cardiol* **44**, 340–348.

Gan C, Lankhaar JW, Marcus JT, Westerhof N, Marques KM, Bronzwaer JG, Boonstra A, Postmus PE & Vonk-Noordegraaf A (2006). Impaired left ventricular filling due to right-to-left ventricular interaction in patients with pulmonary arterial hypertension. *Am J Physiol* **290**, H1528–1533.

Goland S, Czer LSC, Kass RM, De Robertis MA, Mirocha J, Coleman B, Capelli C, Raissi S, Cheng W, Fontana G & Trento A (2007). Pre-existing pulmonary hypertension in patients with end-stage heart failure: Impact on clinical outcome and hemodynamic follow-up after orthotopic heart transplantation. *J Heart Lung Transpl* **26**, 312–318.

Greenberg ML, Uretsky BF, Reddy PS, Bernstein RL, Griffith BP, Hardesty RL, Thompson ME & Bahnson HT (1985). Long-term hemodynamic follow-up of cardiac transplant patients treated with cyclosporine and prednisone. *Circulation* **71**, 487–494.

Gutgesell HP & Rembold CM (1990). Growth of the human heart relative to body surface area. *Am J Cardiol* **65**, 662–668.

Haario H, Laine M, Mira A & Saksman E (2006). DRAM: efficient adaptive MCMC. *Stat Comput* **16**, 339–354.

Hergan K, Schuster A, Fruehwald J, Mair M, Burger R & Topker M (2008). Comparison of left and right ventricular volume measurement using the Simpson's method and the area length method. *Eur J Radiol* **65**, 270–278.

Hudsmith LE, Petersen SE, Francis JM, Robson MD & Neubauer S (2005). Normal human left and right ventricular and left atrial dimensions using steady state free precession magnetic resonance imaging. *J Cardiovasc Magn Reson* **7**, 775–782.

Kelley CT (1999). Iterative Methods for Optimization. *Frontiers in Applied Mathematics*, vol. **18**. Society of Industrial and Applied Mathematics, Philadeplhia, PN, USA.

Klasnja AV, Jakovljevic DG, Barak OF, Gacesa JZP, Lukac DD & Grujic NG (2013). Cardiac power output and its response to exercise in athletes and non-athletes. *Clin Physiol Funct Imaging* **33**, 201–205.

Lumens J, Delhaas T, Kirn B & Arts T (2009). Three-wall segment (TriSeg) model describing mechanics and hemodynamics of ventricular interaction. *Ann Biomed Eng* **37**, 2234–2255.

Marie PY, Angioi M, Carteaux JP, Escanye JM, Mattei S, Tzvetanov K, Claudon O, Hassan N, Danchin N, Karcher G, Bertrand A, Walker PM & Villemot JP (2001). Detection and prediction of acute heart transplant rejection with the myocardial T-2 determination provided by a black-blood magnetic resonance imaging sequence. *J Am Coll Cardiol* **37**, 825–831.

Marquis AD, Arnold A, Dean-Bernhoft C, Carlson BE & Olufsen MS (2018). Practical identifiability and uncertainty quantification of a pulsatile cardiovascular model. *Math Biosci* **304**, 9–24.

Maughan WL, Kallman CH & Shoukas A (1981). The effect of right ventricular filling on the pressure-volume relationship of the ejecting canine left ventricle. *Circ Res* **49**, 382–388.

Nadler SB, Hidalgo JU & Bloch T (1962). Prediction of blood volume in normal human adults. *Surgery* **51**, 224–232.

Nielsens H (2010). smith_chase_nokes_shaw_wake_2004. cellml, pp. CellML version of the cardiovascular systems model presented in Smith et al. *Med Eng Phys* **28**, 131–139, 2004. IUPS Physiome Project., CellML Physiome Model Repository.

Olufsen MS & Ottesen JT (2013). A practical approach to parameter estimation applied to model predicting heart rate regulation. *J Math Biol* **67**, 39–68.

Pope SR, Ellwein LM, Zapata CL, Novak V, Kelley CT & Olufsen MS (2009). Estimation and identification of parameters in a lumped cerebrovascular model. *Math Biosci Eng* **6**, 93–115.

Smith BW, Chase JG, Nokes RI, Shaw GM & Wake G (2004). Minimal haemodynamic system model including ventricular interaction and valve dynamics. *Med Eng Phys* **26**, 131–139.

Smith RC (2013). *Uncertianty Quantification: Theory, Implementation and Applications*, vol. 12. Society for Industrial and Applied Mathematics, Philadelphia, PA, USA.

Stobierska-Dzierzek B, Awad H & Michler RE (2001). The evolving management of acute right-sided heart failure in cardiac transplant recipients. *J Am Coll Cardiol* **38**, 923–931.

Sun JP, Abdalla IA, Asher CR, Greenberg NL, Popovic ZB, Taylor DO, Starling RC, Thomas JD & Garcia MJ (2005). Non-invasive evaluation of orthotopic heart transplant rejection by echocardiography. *J Heart Lung Transpl* **24**, 160–165.

Sundereswaran L, Nagueh SF, Vardan S, Middleton KJ, Zoghbi WA, Quinones MA & Torre-Amione G (1998). Estimation of left and right ventricular filling pressures after heart transplantation by tissue Doppler imaging. *Am J Cardiol* **82**, 352–357.

Tamborini G, Marsan NA, Gripari P, Maffessanti F, Brusoni D, Muratori M, Caiani EG, Fiorentini C & Pepi M (2010). Reference values for right ventricular volumes and ejection fraction with real-time three-dimensional echocardiography: evaluation in a large series of normal subjects. *J Am Soc Echocardiog* **23**, 109–115.

Williams ND, Wind-Willassen O, Wright AA, Program R, Mehlsen J, Ottesen JT & Olufsen MS (2014). Patient-specific modelling of head-up tilt. *Math Med Biol* **31**, 365–392.

Young JB, Leon CA, Short HD, 3rd, Noon GP, Lawrence EC, Whisennand HH, Pratt CM, Goodman DA, Weilbaecher D, Quinones MA, et al (1987). Evolution of hemodynamics after orthotopic heart and heart-lung transplantation: early restrictive patterns persisting in occult fashion. *J Heart Transplant* **6**, 34–43.

Additional information

Data availability statement

All deidentified clinical data that supports the findings of this study are contained in Table 1 of the manuscript. A version of the model implemented in MATLAB (The MathWorks, Inc., Natick, MA) is available at github.com/alcolunga/Heart_Tx_CVS_Model and at https://wp.math.ncsu.edu/cdg/publications/.

Competing interests

The authors of this manuscript have no competing interests or conflict of interest with respect to this study.

Author contributions

Data were acquired through the clinical data repository at the University of Washington Medicine Regional Heart Center. Analysis on the data was performed at the University of Michigan and North Carolina State University. Conception and design: JHG, MSO and BEC. Acquisition of data: KGK, TFD and JHG. Analysis and interpretation: ALC, KGK, NPW, MSO and BEC. Drafting manuscript: ALC, KGK, NPW, JHG, MSO and BEC. Revising manuscript: ALC, NPW, TFD, MSO and BEC. All authors have read and approved the final version of the manuscript. In addition, all authors agree to be accountable for all aspects of the work in ensuring that questions related to the accuracy or integrity of any part of the work are appropriately investigated and resolved. All persons designated as authors qualify for authorship, and all those that qualify for authorship are listed.

Funding

This work is supported by National Institute of Health, National Library of Medicine grant R01 LM011969 (KGK, JHG and BEC), National Institute of Health, National Heart, Lung and Blood Institute R01 HL139813 (BEC), National Science Foundation, Division of Mathematical Sciences 1615820 (MSO), National Science Foundations, Division of Mathematical Sciences Research Training Group 1246991 (NPW and MSO) and The National GEM Consortium, GEM Graduate Fellowship (ALC).

Keywords

computational physiology, heart transplant, patient-specific modeling, right heart catheterization

Supporting information

Additional supporting information may be found online in the Supporting Information section at the end of the article.

Statistical Summary Document